The Astrophysical Journal, 693:1601–1609, 2009 March 10 doi:10.1088/0004-637X/693/2/1601
© 2009. The American Astronomical Society. All rights reserved. Printed in the U.S.A.

PROPAGATION OF NONADIABATIC MAGNETOACOUSTIC WAVES IN A THREADED PROMINENCE WITH MASS FLOWS

R. Soler, R. Oliver, and J. L. Ballester
Departament de Física, Universitat de les Illes Balears, E-07122, Palma de Mallorca, Spain; roberto.soler@uib.es, ramon.oliver@uib.es, joseluis.ballester@uib.es
Received 2008 September 29; accepted 2008 December 4; published 2009 March 10

ABSTRACT

High-resolution observations of solar filaments suggest the presence of groups of prominence threads, i.e., the fine structures of solar prominences, which oscillate coherently (in phase). In addition, mass flows along threads have been often observed. Here, we investigate the effect of mass flows on the collective fast and slow nonadiabatic magnetoacoustic wave modes supported by systems of prominence threads. Prominence fine structures are modeled as parallel, homogeneous, and infinite cylinders embedded in a coronal environment. The magnetic field is uniform and parallel to the axis of threads. Configurations of identical and nonidentical threads are both explored. We apply the *T*-matrix theory of acoustic scattering to obtain the oscillatory frequency and the eigenfunctions of linear magnetosonic disturbances. We find that the existence of wave modes with a collective dynamics, i.e., those that produce significant perturbations in all threads, is only possible when the Doppler-shifted individual frequencies of threads are very similar. This can be only achieved for very particular values of the plasma physical conditions and flow velocities within threads.

Key words: Sun: corona – Sun: magnetic fields – Sun: oscillations – Sun: prominences

Online-only material: color figures

1. INTRODUCTION

Prominences/filaments are fascinating coronal magnetic structures, whose dynamics and properties are not well understood yet. The long life of the so-called quiescent prominences (several weeks) suggests that the cool and dense prominence material is maintained against gravity and thermally shielded from the much hotter and much rarer solar corona by means of some not well known processes. However, it is believed that the magnetic field must play a crucial role in both the support and isolation of prominences. High-resolution observations of solar filaments reveal that they are formed by a myriad of horizontal structures called threads (e.g., Lin et al. 2005), which have been observed in the spines and barbs of both active region and quiescent filaments (Lin et al. 2008). The width of these fine structures is typically in the range 0.″2–0.″6, which is close to the resolution of present-day telescopes, whereas their lengths are between 5″ and 20″ (Lin 2004). Threads are assumed to be the basic substructures of filaments and to be aligned along magnetic field lines. From the point of view of theoretical modeling, prominence threads are interpreted as large coronal magnetic flux tubes, with the denser and cooler (prominence) region located at magnetic field dips that correspond to the observed threads. Although some theoretical works have attempted to model such structures (e.g., Ballester & Priest 1989; Schmitt & Degenhardt 1995; Rempel et al. 1999; Heinzel & Anzer 2006), there are some concerns about their formation and stability that have not been resolved yet.

Small-amplitude oscillations, propagating waves and mass flows are some phenomena usually observed in prominences and prominence threads (see some recent reviews by Oliver & Ballester 2002; Ballester 2006; Banerjee et al. 2007). Periods of small-amplitude prominence oscillations cover a wide range from less than a minute to several hours, and they are usually attenuated in a few periods (Molowny-Horas et al. 1999; Terradas et al. 2002). Focusing on prominence threads, some works have detected oscillations and waves in such fine structures (e.g., Yi et al. 1991; Yi & Engvold 1991; Lin 2004; Okamoto et al. 2007; Lin et al. 2007). In particular, Yi et al. (1991) and Lin et al. (2007) suggested the presence of groups of near threads that moved in phase, which may be a signature of collective oscillations. On the other hand, mass flows along magnetic field lines have been also detected (Zirker et al. 1994, 1998; Lin et al. 2003, 2005), with typical flow velocities of less than 30 km s^{-1} in quiescent prominences, although larger values have been detected in active region prominences (Okamoto et al. 2007). Regarding the presence of flows, a phenomenon that deserves special attention is the existence of the so-called counterstreaming flows, i.e., opposite flows within adjacent threads (Zirker et al. 1998; Lin et al. 2003).

Motivated by the observational evidence, some authors have broached the theoretical investigation of prominence thread oscillations by means of the magnetohydrodynamic (MHD) theory in the $\beta = 0$ approximation. First, some works (Joarder et al. 1997; Díaz et al. 2001, 2003) focused on the study of the ideal MHD oscillatory modes supported by individual nonuniform threads in Cartesian geometry. Later, Díaz et al. (2002) considered a more representative cylindrical thread and obtained more realistic results with respect to the spatial structure of perturbations and the behavior of trapped modes. Subsequently, the attention of authors turned to the study of collective oscillations of groups of threads, and the Cartesian geometry was adopted again for simplicity. Hence, Díaz et al. (2005) investigated the collective fast modes of systems of nonidentical threads and found that the only nonleaky mode corresponds to that in which all threads oscillate in spatial phase. Later, Díaz & Roberts (2006) considered the limit of a periodic array of threads and obtained a similar conclusion. Therefore, these results seem to indicate that all threads within the prominence should oscillate coherently, even if they have different physical properties. However, one must bear in mind that the Cartesian geometry provides quite an unrealistic confinement of perturbations, and

so systems of more realistic cylindrical threads might not show such a clear collective behavior.

The next obvious step is therefore the investigation of oscillatory modes of systems of cylindrical threads. The first approach to a similar problem was done by Luna et al. (2008), who considered a system of two identical, homogeneous cylinders embedded in unlimited corona. Although Luna et al. (2008) applied their results to coronal loops, they are also applicable to prominence threads. These authors numerically found that the system supports four trapped kinklike collective modes. These results have been analytically reobtained by van Doorsselaere et al. (2008), by considering the thin tube approximation and bicylindrical coordinates. Subsequently, Luna et al. (2009) made use of the *T*-matrix theory of acoustic scattering to study the collective oscillations of arbitrary systems of nonidentical cylinders. Although the scattering theory has been previously applied in the solar context (e.g., Bogdan & Zweibel 1987; Keppens 1994), the first application to the study of normal modes of magnetic coronal structures has been performed by Luna et al. (2009). They concluded that, contrary to the Cartesian case of Díaz et al. (2005), the collective behavior of the oscillations diminishes when cylinders with nonidentical densities are considered, the oscillatory modes behaving in practice like individual modes if cylinders with mildly different densities are assumed.

The present study is based on Luna et al. (2009) and applies their technique to the investigation of MHD waves in systems of cylindrical prominence threads. Moreover, we extend their model by considering some effects neglected by them. Here, the more general $\beta \neq 0$ case is considered, allowing us to describe both slow and fast magnetoacoustic modes. In addition, the adiabatic assumption is removed and, following previous papers (Soler et al. 2007, 2008), the effect of radiative losses, thermal conduction and plasma heating is taken into account. The detection of mass flows in prominences has motivated us to include this effect in our study, and so the presence of flows along magnetic field lines is also considered here. Therefore, the present work extends our recent investigation (Soler et al. 2008, hereafter Paper I), which was focused on individual thread oscillations, to the study of collective MHD modes in prominence multithread configurations with mass flows. On the other hand, the longitudinal structure of threads (e.g., Díaz et al. 2002) is neglected in the present investigation. For this reason, the effect of including a longitudinal variation of the plasma physical conditions within threads should be investigated in a future work. Finally, the prominence multithread model developed here could be a useful tool for future seismological applications (similar to that of Terradas et al. 2008).

This paper is organized as follows. The description of the model configuration and the mathematical method is given in Section 2. Then, the results are presented in Section 3. First, the case of two identical prominence threads is investigated in Section 3.1. Later, this study is extended to a configuration of two different threads in Section 3.2. Finally, our conclusion is given in Section 4.

2. MATHEMATICAL METHOD

Our equilibrium system is made of an arbitrary configuration of N homogeneous and unlimited parallel cylinders, representing prominence threads, embedded in an also homogeneous and unbounded coronal medium. Each thread has its own radius, a_j, temperature, T_j, and density, ρ_j, where the subscript j refers to a particular thread. On the other hand, the coronal temperature and density are T_c and ρ_c, respectively. Cylinders are orientated along the z-direction, the (x, y)-plane being perpendicular to their axis. The magnetic field is uniform and also orientated along the z-direction, $\mathbf{B}_j = B_j\hat{\mathbf{e}}_z$ being the magnetic field in the jth thread, and $\mathbf{B}_c = B_c\hat{\mathbf{e}}_z$ in the coronal medium. In addition, steady mass flows are assumed along magnetic field lines, with flow velocities and directions that can be different within threads and in the corona. Thus, $\mathbf{U}_j = U_j\hat{\mathbf{e}}_z$ represents the mass flow in the jth thread, whereas $\mathbf{U}_c = U_c\hat{\mathbf{e}}_z$ corresponds to the coronal flow. For simplicity, in all the following expressions a subscript 0 indicates local equilibrium values, while subscripts j or c denote quantities explicitly computed in the jth thread or in the corona, respectively.

Such as shown in Paper I, linear nonadiabatic magnetoacoustic perturbations are governed by the following equation for the divergence of the velocity perturbation, $\Delta = \nabla \cdot \mathbf{v}_1$,

$$\Upsilon_0^2\left[\Upsilon_0^2 - \left(\tilde{\Lambda}_0^2 + v_{\mathrm{A}0}^2\right)\nabla^2\right]\Delta + \tilde{\Lambda}_0^2 v_{\mathrm{A}0}^2 \frac{\partial^2}{\partial z^2}\nabla^2\Delta = 0, \tag{1}$$

where Υ_0 is the following operator,

$$\Upsilon_0 = \frac{\partial}{\partial t} + U_0\frac{\partial}{\partial z}, \tag{2}$$

while $v_{\mathrm{A}0}^2 = \frac{B_0^2}{\mu\rho_0}$ is the Alfvén speed squared and $\tilde{\Lambda}_0^2$ is the nonadiabatic sound speed squared,

$$\tilde{\Lambda}_0^2 \equiv \frac{c_{\mathrm{s}0}^2}{\gamma}\left[\frac{(\gamma-1)\left(\frac{T_0}{p_0}\kappa_{\parallel 0}k_z^2 + \omega_{T0} - \omega_{\rho 0}\right) + i\gamma\Omega_0}{(\gamma-1)\left(\frac{T_0}{p_0}\kappa_{\parallel 0}k_z^2 + \omega_{T0}\right) + i\Omega_0}\right], \tag{3}$$

$c_{\mathrm{s}0}^2 = \frac{\gamma p_0}{\rho_0}$ and γ being the adiabatic sound speed squared and the adiabatic ratio, respectively. Terms with $\kappa_{\parallel 0}$, $\omega_{\rho 0}$, and ω_{T0} are related to nonadiabatic mechanisms, i.e. radiative losses, thermal conduction, and heating (see Paper I for details). Finally, Ω_0 is the Doppler-shifted frequency (Terra-Homem et al. 2003),

$$\Omega_0 = \omega - k_z U_0, \tag{4}$$

where ω is the oscillatory frequency and k_z is the longitudinal wavenumber. Considering cylindrical coordinates, namely r, φ, and z for the radial, azimuthal, and longitudinal coordinates, respectively, we can write Δ in the following form,

$$\Delta = \psi(r, \varphi)\exp(i\omega t - ik_z z), \tag{5}$$

where the function $\psi(r, \varphi)$ contains the full radial and azimuthal dependence. By inserting this last expression into Equation (1), the following Helmholtz equation is obtained,

$$\nabla_{r\varphi}^2\psi(r, \varphi) + m_0^2\psi(r, \varphi) = 0, \tag{6}$$

where $\nabla_{r\varphi}^2$ is the Laplacian operator for the r and φ coordinates, and

$$m_0^2 = \frac{\left(\Omega_0^2 - k_z^2 v_{\mathrm{A}0}^2\right)\left(\Omega_0^2 - k_z^2\tilde{\Lambda}_0^2\right)}{\left(v_{\mathrm{A}0}^2 + \tilde{\Lambda}_0^2\right)\left(\Omega_0^2 - k_z^2\tilde{c}_{\mathrm{T}0}^2\right)}, \tag{7}$$

$$\tilde{c}_{\mathrm{T}0}^2 \equiv \frac{v_{\mathrm{A}0}^2\tilde{\Lambda}_0^2}{v_{\mathrm{A}0}^2 + \tilde{\Lambda}_0^2}, \tag{8}$$

are the radial wave number and the nonadiabatic tube speed squared, respectively. Moreover, due to the presence of nonideal terms m_0^2 is a complex quantity. Since nonadiabatic

mechanisms produce a small correction to the adiabatic wave modes, $|\Re(m_0^2)| > |\Im(m_0^2)|$ and the dominant wave character depend on the sign of $\Re(m_0^2)$. Here, we investigate nonleaky modes, which are given by $\Re(m_c^2) < 0$. We impose no restriction on the wave character within threads.

In order to solve Equation (6), we consider the technique developed by Luna et al. (2009) based on the study of wave modes of an arbitrary configuration of cylinders by means of the T-matrix theory of acoustic scattering. The novelty with respect to the work of Luna et al. (2009) is that the method is applied here to solve a Helmholtz equation for the divergence of the velocity perturbation (our Equation (1)) whereas Luna et al. (2009) considered an equation for the total pressure perturbation in the $\beta = 0$ approximation (their Equation (1)). The present approach allows us to study the more general $\beta \neq 0$ case, therefore slow modes are also described. In addition, nonadiabatic effects and mass flows are easily included in our formalism. However, the rest of the technique is absolutely equivalent to that of Luna et al. (2009), and therefore the reader is referred to their work for an extensive explanation of the mathematical technique (see also an equivalent formalism in Bogdan & Cattaneo 1989). We next give a brief summary of the method.

The main difference between our application and that of Luna et al. (2009) is in the definition of the T-matrix elements. These elements are obtained by imposing appropriate boundary conditions at the edge of threads, i.e., at $|\mathbf{r} - \mathbf{r}_j| = a_j$, where $\mathbf{r}_j$ is the radial vector corresponding to the position of the jth thread center with respect to the origin of coordinates. In our case, these boundary conditions are the continuity of the total pressure perturbation, $p_{\rm T}$, and the Lagrangian radial displacement, $\xi_r = -i\,v_r/\Omega_0$. Expressions for these quantities as functions of Δ and its derivative are,

$$p_{\rm T} = i\rho_0 \frac{\left(\Omega_0^2 - k_z^2\tilde{\Lambda}_0^2\right)\left(\Omega_0^2 - k_z^2 v_{\rm A0}^2\right)}{\Omega_0^3 m_0^2}\Delta, \tag{9}$$

$$\xi_r = i\,\frac{\left(\Omega_0^2 - k_z^2\tilde{\Lambda}_0^2\right)}{\Omega_0^3 m_0^2}\frac{\partial\Delta}{\partial r}. \tag{10}$$

Expressions for the rest of perturbations are given in Appendix A of Paper I. Thus, in our case the T-matrix elements have the following form,

$$\begin{aligned} T^j_{mm} = &\left\{m_c\rho_j\left(\Omega_j^2 - k_z^2 v_{{\rm A}_j}^2\right)J_m(m_j a_j)J'_m(m_c a_j)\right.\\ &\left. - m_j\rho_c\left(\Omega_c^2 - k_z^2 v_{{\rm A}_c}^2\right)J_m(m_c a_j)J'_m(m_j a_j)\right\}\Big/\\ &\left\{m_c\rho_j\left(\Omega_j^2 - k_z^2 v_{{\rm A}_j}^2\right)J_m(m_j a_j)H'^{(1)}_m(m_c a_j)\right.\\ &\left. - m_j\rho_c\left(\Omega_c^2 - k_z^2 v_{{\rm A}_c}^2\right)H^{(1)}_m(m_c a_j)J'_m(m_j a_j)\right\}, \end{aligned} \tag{11}$$

where $H^{(1)}_m$ and J_m are the Hankel function of the first kind and the Bessel function of order m, respectively, while the prime denotes the derivative taken with respect to r. Note that the denominator of T^j_{mm} vanishes at the normal mode frequencies of an individual thread. This can be easily checked by comparing it with the dispersion relation of a single thread, see Equation (19) of Paper I, in which Bessel K_m functions are used instead of Hankel functions. The equivalence between both kinds of functions is given in Abramowitz & Stegun (1972). Thus, following Luna et al. (2009), the internal $\psi\,(r, \varphi)$ field of the jth thread is

$$\psi^j_{\rm int}(r,\varphi) = \sum_{m=-\infty}^{\infty} A^j_m J_m(m_j|\mathbf{r} - \mathbf{r}_j|)e^{im\varphi_j}, \tag{12}$$

whereas the external net field is

$$\psi_{\rm ext}(r,\varphi) = -\sum_j \sum_{m=-\infty}^{\infty} 2\alpha^j_{2,m} T^j_{mm} H^{(1)}_m(m_c|\mathbf{r} - \mathbf{r}_j|)e^{im\varphi_j}, \tag{13}$$

where φ_j is the azimuthal angle corresponding to the position of the jth thread center with respect to the origin of coordinates, and $\alpha^j_{2,m}$ and A^j_m are constants. Equations (12) and (13) allow us to construct the spatial distribution of Δ. Subsequently, the rest of the perturbations can be obtained. Finally, the constants $\alpha^j_{2,m}$ form a homogeneous system of linear algebraic equations,

$$\alpha^j_{2,m} + \sum_{k\neq j}\sum_{n=-\infty}^{\infty} T^k_{nn}\alpha^k_{2,n} H^{(1)}_{n-m}(m_c|\mathbf{r}_j - \mathbf{r}_k|)e^{i(n-m)\varphi_{jk}} = 0, \tag{14}$$

for $-\infty < m < \infty$. Once both integers m and n are truncated to a finite number of terms, the nontrivial (i.e., nonzero) solution of system in Equation (14) gives us a dispersion relation for the oscillatory frequency, ω, which is enclosed in the definitions of m_j and m_c.

In the following sections, we apply the method for obtaining the oscillatory frequency and the spatial distribution of perturbations of the wave modes supported by prominence thread configurations. We assume that k_z is real, so a complex frequency is obtained, namely $\omega = \omega_{\rm R} + i\omega_{\rm I}$. The imaginary part of the frequency appears due to the presence of nonadiabatic mechanisms. The oscillatory period, P, and the damping time, $\tau_{\rm D}$, are related to the frequency as follows,

$$P = \frac{2\pi}{|\omega_{\rm R}|}, \qquad \tau_{\rm D} = \frac{1}{\omega_{\rm I}}. \tag{15}$$

3. RESULTS

3.1. Configuration of Two Identical Threads

Now, we consider a configuration of two identical threads (see Figure 1). Their physical conditions are typical of prominences ($T_1 = T_2 = 8000$ K, $\rho_1 = \rho_2 = 5 \times 10^{-11}$ kg m^{-3}) while the coronal temperature and density are $T_{\rm c} = 10^6$ K and $\rho_{\rm c} = 2.5 \times 10^{-13}$ kg m^{-3}, respectively. Their radii are $a_1 = a_2 = a = 30$ km, and the distance between centers is $d = 4a = 120$ km. The magnetic field strength is 5 G everywhere. The flow velocity inside the cylinders is denoted by U_1 and U_2, respectively, whereas the flow velocity in the coronal medium is $U_{\rm c}$. Unless otherwise stated, these physical conditions are used in all calculations.

As mentioned in Section 1, the observed width of the threads is less than 0.″3, which is very close to the resolution of present-day telescopes. Therefore, it is possible that thinner threads could exist in prominences, which may not be well resolved now but they should be observable by future instruments with a higher spatial resolution. This is the reason for considering here thread radii slightly smaller than those currently observed. On the other hand, for typical wavelengths of prominence oscillations, the wave behavior is in practice independent of the value of the radius, i.e., the "thin tube" regime, and therefore the very value of the radius is almost irrelevant for this investigation.

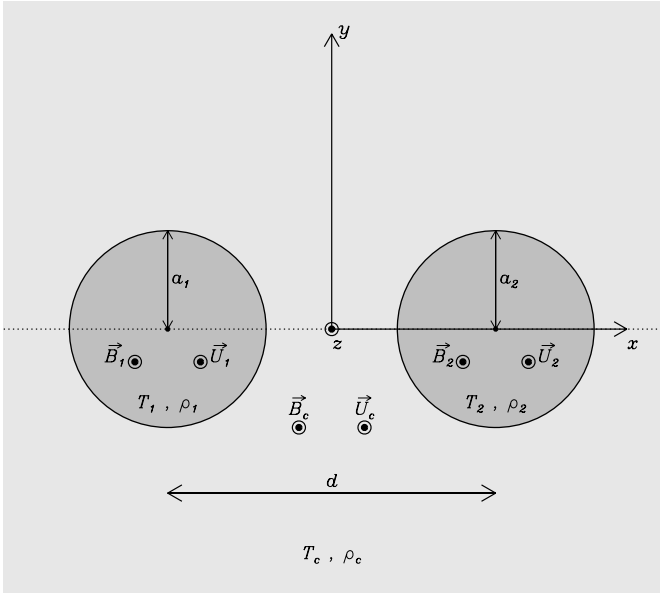

Figure 1. Scheme in the (x, y)-plane of the model considered in Section 3.1. The z-axis is perpendicular to the plane of the figure and points toward the reader.

3.1.1. Wave Modes in the Absence of Flow

First, we consider no flow in the equilibrium, i.e., $U_1 = U_2 = U_c = 0$. We fix the longitudinal wavenumber to $k_z a = 10^{-2}$, which corresponds to a wavelength within the typically observed range. In addition to the four kink modes described by Luna et al. (2008), i.e., the S_x, A_x, S_y, and A_y modes, where S or A denote symmetry or antisymmetry of the total pressure perturbation with respect to the (y, z)-plane, and the subscripts refer to the main direction of polarization of motions, we also find two more fundamental collective wave modes (one symmetric and one antisymmetric) mainly polarized along the z-direction, which we call S_z and A_z modes following the notation of Luna et al. (2008). These new solutions correspond to slow modes that are absent in the investigation of Luna et al. (2008) due to their $\beta = 0$ approximation. As was stated by Luna et al. (2009), a collective wave mode is the result of a coupling between individual modes. The reader must be aware that in the present work we indistinctly use both expressions, i.e., collective modes and coupled modes, to refer to wave solutions whose perturbations have significant amplitudes in both threads.

The total pressure perturbation field, p_T, and the transverse Lagrangian displacement vector-field, $\xi_\perp$, corresponding to the six fundamental modes are displayed in Figure 2. On the other hand, Figure 3 displays a cut of the Cartesian components of the Lagrangian displacement (ξ_x, ξ_y, and ξ_z) at $y = 0$, again for these six solutions. For simplicity, only the real part of these quantities are plotted in both figures, since their imaginary parts are equivalent. One can see in Figure 3 that the amplitude of the longitudinal (magnetic field aligned) Lagrangian displacement, ξ_z, of the S_z and A_z modes is much larger than the amplitude of transverse displacements, ξ_x and ξ_y, such as corresponds to slow modes in $\beta < 1$ homogeneous media, while the contrary occurs for the S_x, A_x, S_y, and A_y fast kink solutions.

Next, Figure 4(a) displays the ratio of the real part of the frequency of the four kink solutions to the frequency of the individual kink mode, ω_k (from Paper I), as a function of the distance between the center of cylinders, d. This Figure is equivalent to Figure 3 of Luna et al. (2008) and, in agreement with them, one can see that the smaller the distance between centers, the larger the interaction between threads and so the larger the separation between frequencies. The frequency of collective kink modes is almost identical to the individual kink frequency for a distance between threads larger than 6 or 7 radii. Therefore, we expect the collective behavior of oscillations to be stronger for smaller distances. Since the present investigation is focused on the collective behavior of oscillations, we consider in the following sections small enough distances in order to be in the collective regime. For larger distances, the interaction between threads is much weaker and we expect oscillations to be almost individual. On the other hand, Figure 4(b) shows the ratio of the damping time to the period of the four kink modes as a function of d. We see that the damping times are between 4 and 7 orders of magnitude larger than their corresponding periods. Therefore, dissipation by nonadiabatic mechanisms cannot be responsible for the observed damping times of transverse thread oscillations, as was pointed out in Paper I. Recently, Arregui et al. (2008) found that the mechanism of resonant absorption can provide kink mode damping times compatible with those observed.

Regarding slow modes, Figure 5(a) displays the ratio of the real part of the frequency of the S_z and A_z solutions to the frequency of the individual slow mode, ω_s (from Paper I). One can see that the frequencies of the S_z and A_z modes are almost identical to the individual slow mode frequency, and so the strength of the interaction is almost independent of the distance between cylinders. This is consistent with the fact that transverse motions (responsible for the interaction between threads) are not significant for slowlike modes in comparison with their longitudinal motions. Therefore, the S_z and A_z modes essentially behave as individual slow modes, contrary to kink modes, which display a more significant collective behavior. Finally, Figure 5(b) shows τ_D/P corresponding to the S_z and A_z solutions versus d. One sees that both slow modes are efficiently attenuated by nonadiabatic mechanisms, with $\tau_D/P \approx 5$, which is in agreement with previous studies Soler et al. (2007, 2008) and consistent with observations.

3.1.2. Effect of Steady Mass Flows on the Collective Behavior of Wave Modes

The aim of the present section is to assess the effect of flows on the behavior of collective modes. With no loss of generality, we assume no flow in the corona, i.e., $U_c = 0$. On the other hand, the flow velocities in both cylinders, namely U_1 and U_2, are free parameters. We vary these flow velocities between -30 km s^{-1} and 30 km s^{-1}, which correspond to the range of typically observed flow velocities in filament threads (e.g., Lin et al. 2003). These flow velocities are below the critical value that determines the apparition of the Kelvin–Helmholtz instability (see details in Holzwarth et al. 2007). In our configuration, a positive flow velocity means that the mass is flowing toward the positive z-direction, whereas the contrary is for negative flow velocities. From Paper I (see also Terra-Homem et al. 2003) we know that the symmetry between waves whose propagation is parallel ($\omega_R > 0$) or antiparallel ($\omega_R < 0$) with respect to magnetic field lines is broken by the presence of flows. Hence, we must take into account the direction of wave propagation in order to perform a correct description of the wave behavior. Following Paper I, we call parallel waves those solutions with $\omega_R > 0$, while antiparallel waves are solutions with $\omega_R < 0$.

We begin this investigation with transverse modes. First, we assume $U_1 = 20$ km s^{-1} and study the behavior of the oscillatory frequency when U_2 varies (see Figure 6). Since frequencies are

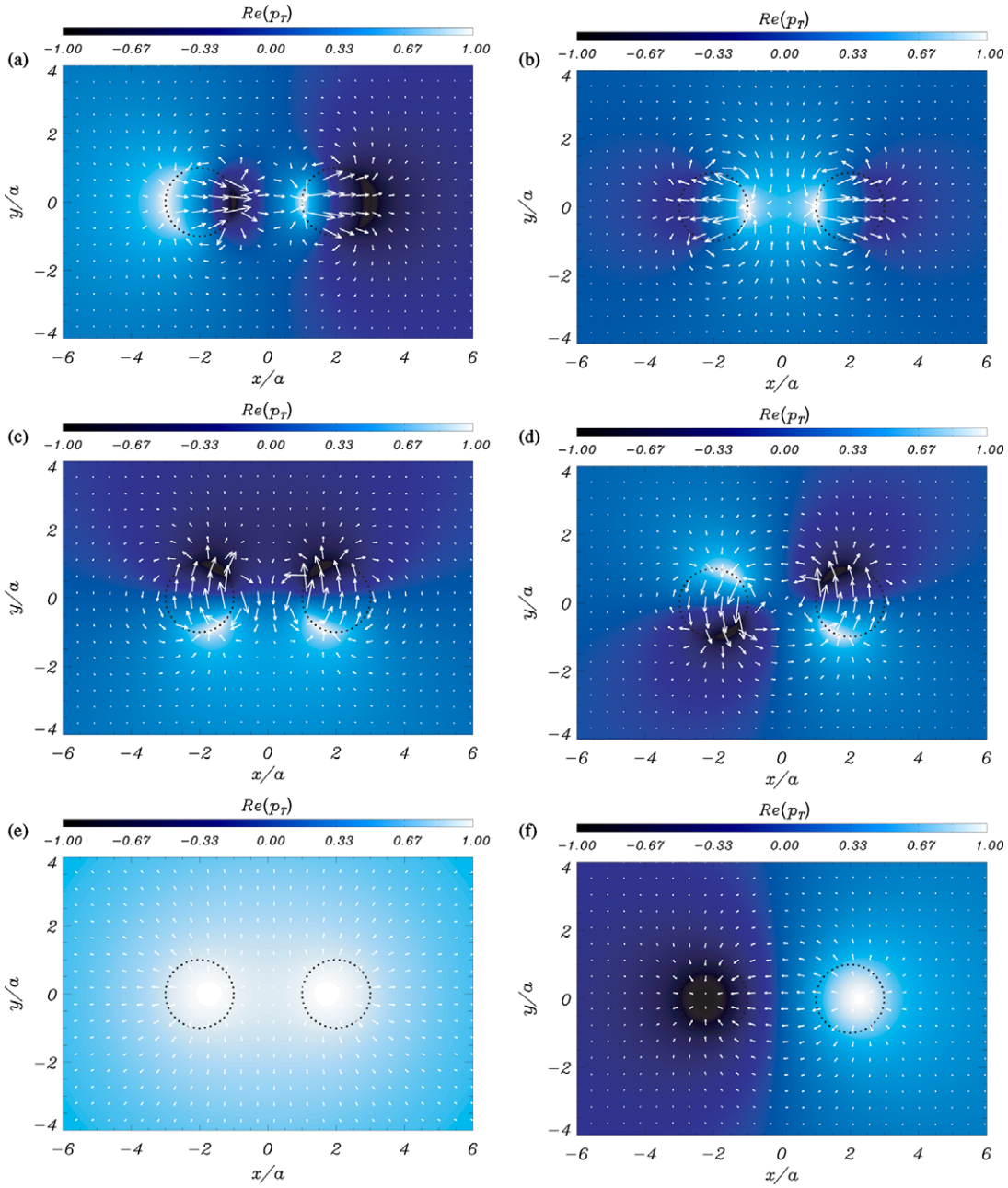

Figure 2. Real part of the total pressure perturbation field (contour plot in arbitrary units) and the transverse Lagrangian displacement vector field (arrows) plotted in the (x, y)-plane corresponding to the wave modes (*a*) S_x, (*b*) A_x, (*c*) S_y, (*d*) A_y, (*e*) S_z, and (*f*) A_z in the absence of flows for a separation between threads $d = 4a$ and a longitudinal wavenumber $k_z a = 10^{-2}$. The location of prominence threads is denoted by dotted circles.

(A color version of this figure is available in the online journal.)

almost degenerate and, therefore, almost indiscernible if they are plotted together, we use the notation of van Doorsselaere et al. (2008) and call low-frequency modes the S_x and A_y solutions, while high-frequency modes refer to A_x and S_y solutions. In addition, we restrict ourselves to parallel propagation because the argumentation can be easily extended to antiparallel waves. To understand the asymptotic behavior of frequencies in Figure 6, we define the following Doppler-shifted individual kink frequencies:

$$\Omega_{k1} = \omega_k + U_1 k_z, \tag{16}$$

$$\Omega_{k2} = \omega_k + U_2 k_z. \tag{17}$$

Since U_1 is fixed, Ω_{k1} is a horizontal line in Figure 6, whereas Ω_{k2} is linear with U_2.

Three interesting situations have been pointed by means of small letters from *a* to *c* in Figure 6. Each of these letters also corresponds to a panel of Figure 7 in which the total pressure perturbation field of the S_x mode is plotted. The three different situations are commented in detail next (remember that in all cases $U_1 = 20$ km s^{-1}).

1. $U_2 = -10$ km s^{-1} ($U_2 < U_1$). This corresponds to a situation of counterstreaming flows. From Figure 6 we see that the frequency of low-frequency modes is close to Ω_{k2}, whereas that of high-frequency solutions is near Ω_{k1}. Thus, these solutions do not interact with each other and low-frequency (high-frequency) solutions are related to individual oscillations of the second (first) thread. This is verified by looking at the total pressure perturbation field

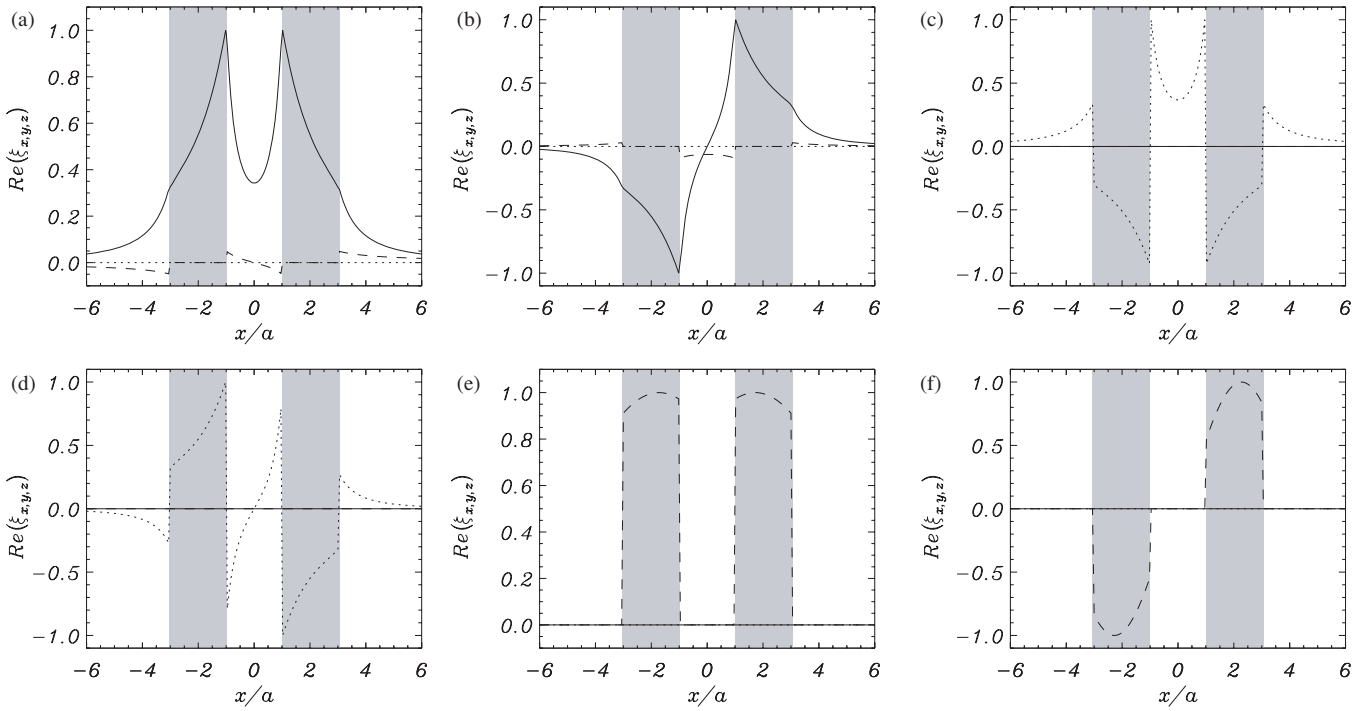

Figure 3. Cut at $y = 0$, $z = 0$ of the real parts (in arbitrary units) of the Cartesian components of the Lagrangian displacement: ξ_x (solid line), ξ_y (dotted line), and ξ_z (dashed line), corresponding to the wave modes (*a*) S_x, (*b*) A_x, (*c*) S_y, (*d*) A_y, (*e*) S_z, and (*f*) A_z for the same conditions of Figure 2. The shaded regions show the location of threads. Note that neither ξ_y nor ξ_z is continuous at the edges of threads.

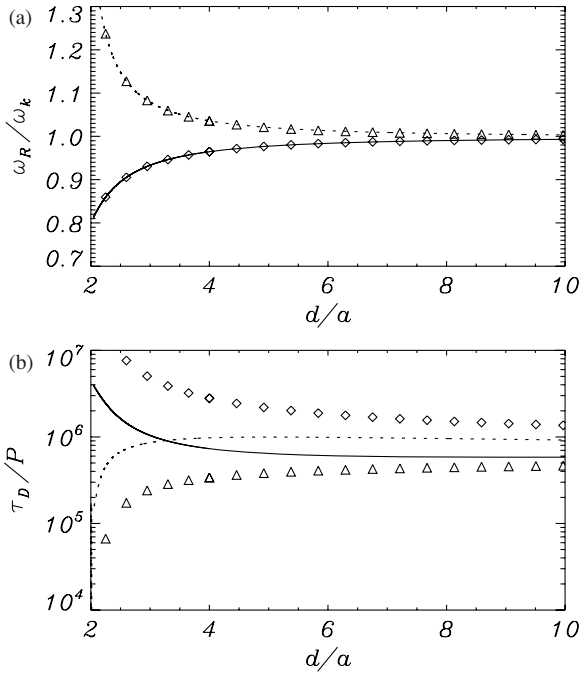

Figure 4. (*a*) Ratio of the real part of frequency, ω_R, of the S_x (solid line), A_x (dotted line), S_y (triangles), and A_y (diamonds) wave modes to the frequency of the individual kink mode, ω_k, as a function of the distance between centers. (*b*) Ratio of the damping time to the period vs. the distance between centers. Line styles are the same as in panel (*a*).

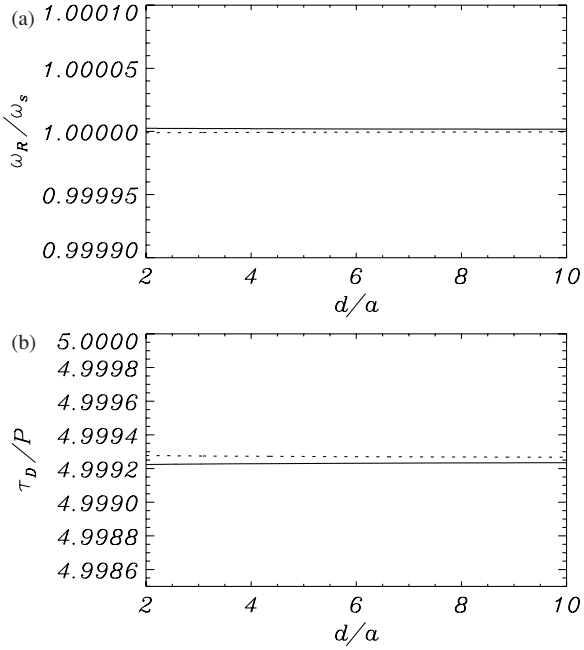

Figure 5. (*a*) Ratio of the real part of frequency, ω_R, of the S_z (solid line) and A_z (dotted line) wave modes to the frequency of the individual slow mode, ω_s, as a function of the distance between centers. (*b*) Ratio of the damping time to the period vs. the distance between centers. Line styles are the same as in panel (*a*).

in Figure 7(a), which shows that only the second thread is significantly perturbed. Therefore, for an external observer this situation corresponds in practice to an individual thread oscillation.

2. $U_2 = 20$ km s^{-1} ($U_2 = U_1$). The flow velocities and their directions are equal in both threads. In such a situation, low- and high-frequency modes couple. At the coupling, an avoided crossing of the solid and dashed lines is seen in Figure 6. Because of this coupling solutions are related no more to oscillations of an individual thread but they are now collective and, for this reason, Figure 7(b) shows a significant pressure perturbation in both threads.

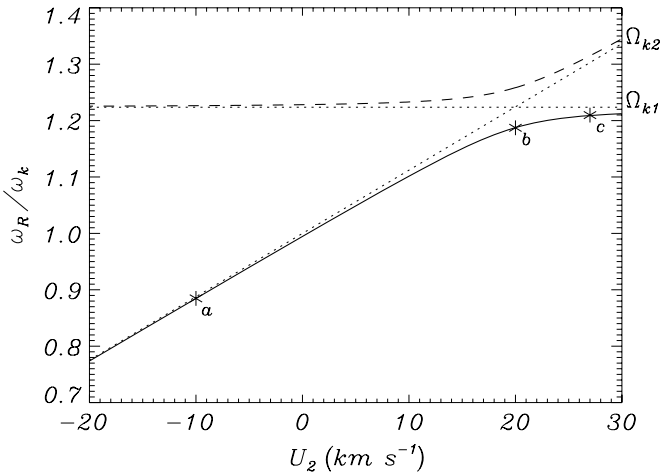

Figure 6. Ratio of the real part of the frequency, ω_R, to the individual kink frequency, ω_k, as a function of U_2 for $U_1 = 20$ km s^{-1}. The solid line corresponds to parallel low-frequency modes (S_x and A_y) while the dashed line corresponds to parallel high-frequency solutions (A_x and S_y). Dotted lines correspond to the Doppler-shifted individual kink frequencies of the threads, Ω_{k1} and Ω_{k2}. The small letters next to the solid line refer to particular situations studied in the text.

3. $U_2 = 27$ km s^{-1} ($U_2 > U_1$). This case is the opposite of situation 1. Therefore, in practice the present situation corresponds again to an individual thread oscillation.

Our argumentation is supported by Figure 8, which displays the amplitude of the transverse Lagrangian displacement, $\xi_\perp$, at the center of the second thread as a function of U_2, for parallel and antiparallel kinklike waves. The displacement amplitude at the center of the first thread is always set equal to unity. The three previously commented situations have been pointed again in Figure 8. We clearly see that the displacement amplitude is only comparable in both threads, and so their dynamics is collective, when their flow velocities are similar.

Next we turn our attention to slow modes. The behavior of the S_z and A_z modes is like that of low- and high-frequency kinklike solutions, so we comment them in short for the sake of simplicity. S_z and A_z solutions can only be considered collective when the flow velocity is the same in both threads because, in such a case, the S_z and A_z modes couple. If different flows within the threads are considered, the S_z and A_z slow modes lose their collective aspect and their frequencies are very close to the Doppler-shifted individual slow frequencies,

$$\Omega_{s1} = \omega_s + U_1 k_z, \tag{18}$$

$$\Omega_{s2} = \omega_s + U_2 k_z. \tag{19}$$

Then, the S_z and A_z solutions behave like individual slow modes. It is worth mentioning that the coupling between slow modes is much more sensible to the flow velocities in comparison with fast modes, and the S_z and A_z solutions quickly decouple if U_1 and U_2 slightly differ. An example of this behavior is seen in Figure 9, which displays the total pressure perturbation field of the A_z mode for $U_1 - U_2 = 10^{-3}$ km s^{-1}. Although the difference of the flow velocities is insignificant, one can see that in this situation the A_z mode essentially behaves as the individual slow mode of the second thread.

The main idea behind these results is that fast or slow wave modes with a collective appearance (i.e., modes with a similar displacement amplitude within all threads) are only possible when the Doppler-shifted individual kink (Equations (16) and (17)) or slow (Equations (18) and (19)) frequencies are similar in both threads. In a system of identical threads, this can only be achieved by considering the same flow velocities within all threads, since all of them have the same individual kink and slow frequencies. However, if threads with different physical properties are considered (i.e., different individual frequencies), it is possible that the coupling may occur for different flow velocities. This is explored in the next section.

3.2. Configuration of Two Threads with Different Physical Properties

Here we consider a system of two nonidentical threads and focus first on kink modes. From Section 3.1 we expect that collective kink motions occur when the Doppler-shifted individual kink frequencies of both threads coincide. The relation between flow velocities U_1 and U_2 for which the coupling takes place can be easily estimated from the equation,

$$\omega_{k1} + U_1 k_z \approx \omega_{k2} + U_2 k_z. \tag{20}$$

Note that the individual kink frequency of each thread is different, i.e., $\omega_{k1} \neq \omega_{k2}$. Then, the relation between flow velocities at the coupling is,

$$U_1 - U_2 \approx \frac{\omega_{k2} - \omega_{k1}}{k_z}. \tag{21}$$

This last expression can be simplified by considering the approximate expression for the kink frequency in the long-wavelength limit,

$$\omega_{ki} \approx \pm\sqrt{\frac{2}{1+\rho_c/\rho_i}}\, v_{Ai} k_z \approx \pm\sqrt{2}\, v_{Ai} k_z, \tag{22}$$

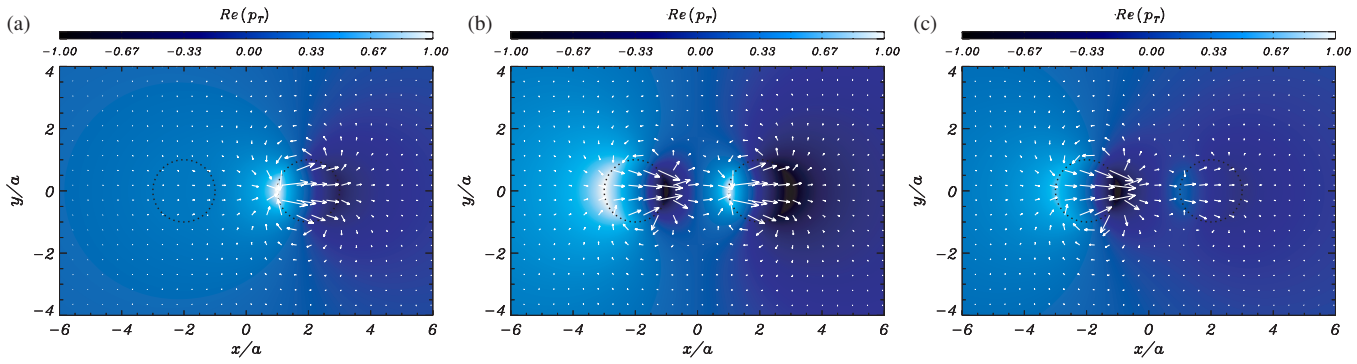

Figure 7. Real part of the total pressure perturbation field (contour plot in arbitrary units) and the transverse Lagrangian displacement vector field (arrows) plotted in the (x, y)-plane corresponding to the parallel S_x mode for (*a*) $U_2 = -10$ km s^{-1}, (*b*) $U_2 = 20$ km s^{-1}, and (*c*) $U_2 = 27$ km s^{-1}. In all cases $U_1 = 20$ km s^{-1}.
(A color version of this figure is available in the online journal.)

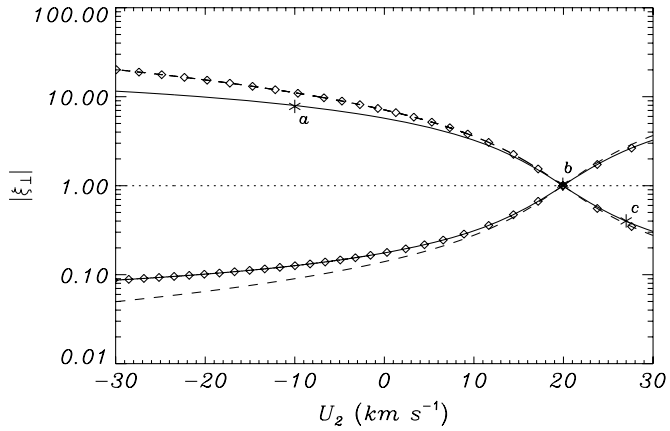

Figure 8. Amplitude (in arbitrary units) of the transverse Lagrangian displacement, $\xi_\perp$, at the center of the second thread as a function of U_2. The amplitude displacement in the first thread center is fixed to unity (dotted line) and the flow velocity is $U_1 = 20$ km s^{-1}. Solid lines correspond to low-frequency kink modes (S_x and A_y), while dashed lines correspond to high-frequency kink solutions (A_x and S_y). Lines without symbols are for parallel waves whereas diamonds indicate antiparallel propagation. Small letters refer to the particular situations discussed in the text.

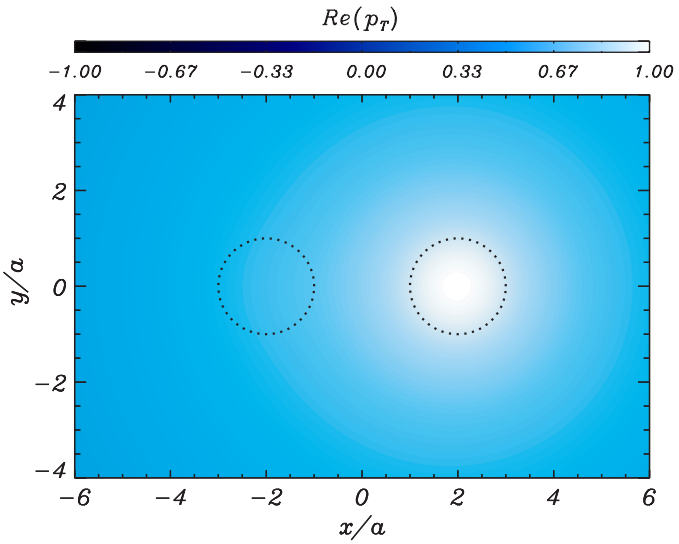

Figure 9. Real part of the total pressure perturbation field plotted in the (x, y)-plane corresponding to the parallel A_z slow mode for a difference between flow velocities of $U_1 - U_2 = 10^{-3}$ km s^{-1}.

(A color version of this figure is available in the online journal.)

for $i = 1, 2$, where the + sign is for parallel waves and the − sign is for antiparallel propagation. Then, one finally obtains

$$U_1 - U_2 \approx \pm\sqrt{2}\,(v_{A2} - v_{A1})\,, \tag{23}$$

where the meaning of the + and − signs is the same as before. In the case of identical threads, $v_{A1} = v_{A2}$ and so $U_1 - U_2 = 0$. Thus the flow velocity must be the same in both threads to obtain collective motions, as we concluded in Section 3.1. An equivalent analysis can be performed for slow modes and one obtains

$$U_1 - U_2 \approx \pm\,(c_{s2} - c_{s1})\,. \tag{24}$$

In general, the coupling between slow modes occurs at different flow velocities than the coupling between kink modes. This makes the simultaneous existence of collective slow and kink solutions in systems of nonidentical threads difficult.

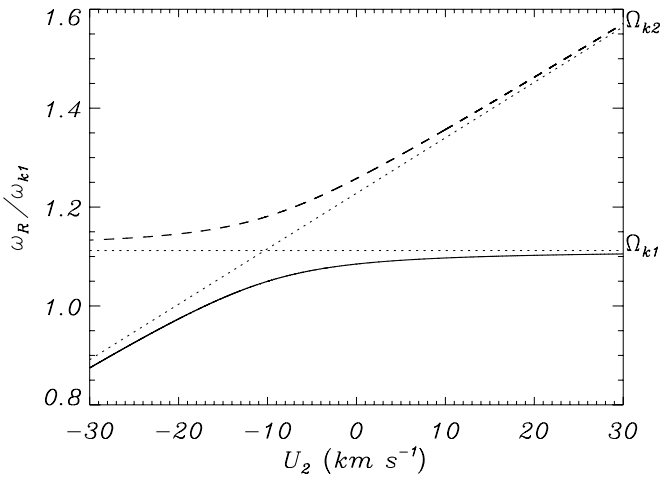

Figure 10. Same as Figure 6 but for the particular configuration studied in Section 3.2.

Next, we assume a particular configuration of two nonidentical threads in order to verify the later argumentation. Thread radii are $a_1 = 30$ km and $a_2 = 45$ km, whereas their physical properties are $T_1 = 8000$ K, $\rho_1 = 5 \times 10^{-11}$ kg m^{-3}, and $T_2 = 12000$ K, $\rho_2 = 3.33 \times 10^{-11}$ kg m^{-3}. Coronal conditions are those taken in Section 3.1 (i.e., $T_c = 10^6$ K, $\rho_c = 2.5 \times 10^{-13}$ kg m^{-3}). The magnetic field strength is 5 G everywhere and the distance between the thread centers is $d = 120$ km. We assume $U_1 = 10$ km s^{-1}. In the present case, also four kinklike solutions are present, which are grouped in two almost degenerate couples. For this reason, we again refer to them as low- and high-frequency kink solutions. Their frequency as a function of U_2 is displayed in Figure 10. At first sight, we see that solutions couple for a particular value of U_2, as expected. Applying Equation (23), and considering that $v_{A1} = 63.08$ km s^{-1} and $v_{A2} = 77.29$ km s^{-1}, we obtain $U_1 - U_2 \approx \pm 20.10$ km s^{-1}, and since $U_1 = 10$ km s^{-1}, we get $U_2 \approx -10.10$ km s^{-1} for parallel propagation. We see that the approximate value of U_2 obtained from Equation (23) is in good agreement with Figure 10. In addition, we obtain that for parallel propagation collective dynamics appear in a situation of counterstreaming (opposite) flows. This result is of special relevance because counterstreaming flows have been detected in prominences (Zirker et al. 1998; Lin et al. 2003) and might play a crucial role in the collective behavior of oscillations. On the contrary, in the antiparallel propagation case we obtain $U_2 \approx 30.10$ km s^{-1} from Equation (23), and so both flows are in the same direction and quite a large value of U_2 is obtained in comparison with the parallel propagation case.

Regarding slow modes, considering that $c_{s1} = 11.76$ km s^{-1} and $c_{s2} = 14.40$ km s^{-1}, Equation (24) gives $U_2 \approx 7.36$ km s^{-1} for parallel propagation and $U_2 \approx 12.64$ km s^{-1} for antiparallel waves. Note that in our particular example the flow velocities needed for the coupling situation are realistic and within the range of typically observed velocities. However, if threads with very different physical properties and, therefore, with very different Alfvén and sound speeds are considered, the coupling flow velocities could be larger than the observed values. This means that the conditions necessary for collective oscillations of systems of threads with very different temperatures and/or densities may not be realistic in the context of solar prominences.

4. CONCLUSION

In this work, we have assessed the effect of mass flows on the collective behavior of slow and fast kink magnetosonic wave

modes in systems of prominence threads. We have seen that the relation between the individual Alfvén (sound) speed of threads is the relevant parameter which determines whether the behavior of kink (slow) modes is collective or individual. In the absence of flows and when the Alfvén speeds of threads are similar, kink modes are of collective type. On the contrary, perturbations are confined within an individual thread if the Alfvén speeds differ. In the case of slow modes, the conclusion is equivalent but replacing the Alfvén speeds by the sound speeds of threads. On the other hand, when flows are present in the equilibrium, one can find again collective motions even in systems of nonidentical threads by considering appropriate flow velocities. These velocities are within the observed values if threads with not too different temperatures and densities are assumed. However, since the flow velocities required for collective oscillations must take very particular values, such a special situation may rarely occur in real prominences.

Therefore, if coherent oscillations of groups of threads are observed in prominences (e.g., Lin et al. 2007), we conclude that either the physical properties and flow velocities of all oscillating threads are quite similar or, if they have different properties, the flow velocities within threads are the appropriate ones to allow collective motions. From our point of view, the first option is the most probable one since the flow velocities required in the second case correspond to a very peculiar situation. This conclusion has important repercussions for future prominence seismological applications, in the sense that if collective oscillations are observed in large areas of a prominence, threads in such regions should possess very similar temperatures, densities, and magnetic field strengths

Here, we have only considered two-thread systems, but the method can be applied to an arbitrary multithread configuration. So, the model developed here could be used to perform seismological studies of large ensembles of prominence threads if future observations provide with positions and physical parameters of such systems.

R.S. is very grateful to M. Luna for his useful comments and fruitful discussions during the preparation of the paper. The authors acknowledge the financial support received from the Spanish MICINN and the Conselleria d'Economia, Hisenda i Innovació of the CAIB under Grants No. AYA2006-07637 and PCTIB-2005GC3-03, respectively. R.S. also thanks the Conselleria d'Economia, Hisenda i Innovació for a fellowship. Finally, the authors acknowledge the International Space Science Institute teams "Coronal waves and Oscillations" and "Spectroscopy and Imaging of quiescent and eruptive solar prominences from space" for useful discussions.

REFERENCES

Abramowitz, M., & Stegun, I. A. 1972, Handbook of Mathematical Functions (New York: Dover Publications)
Arregui, I., Terradas, J., Oliver, R., & Ballester, J. L. 2008, ApJ, 682, L141
Ballester, J. L., & Priest, E. R. 1989, A&A, 225, 213
Ballester, J. L. 2006, Phil. Trans. R. Soc. A, 364, 405
Banerjee, D., Erdélyi, R., Oliver, R., & O'Shea, E. 2007, Sol. Phys., 246, 3
Bogdan, T. J., & Zweibel, E. G. 1987, ApJ, 312, 444
Bogdan, T. J., & Cattaneao, F. 1989, ApJ, 342, 545
Díaz, A. J., Oliver, R., & Ballester, J. L. 2002, ApJ, 580, 550
Díaz, A. J., Oliver, R., & Ballester, J. L. 2003, A&A, 402, 781
Díaz, A. J., Oliver, R., & Ballester, J. L. 2005, A&A, 440, 1167
Díaz, A. J., Oliver, R., Erdélyi, R., & Ballester, J. L. 2001, A&A, 379, 1083
Díaz, A. J., & Roberts, B. 2006, Sol. Phys., 236, 111
Heinzel, P., & Anzer, U. 2006, ApJ, 643, L65
Holzwarth, V., Schmitt, D., & Schüssler, M. 2007, A&A, 469, 11
Joarder, P. S., Nakariakov, V. M., & Roberts, B. 1997, Sol. Phys., 173, 81
Keppens, R. 1994, PhD thesis, Katholieke Univ. Leuven
Lin, Y. 2004, PhD thesis, Univ. of Oslo
Lin, Y., Engvold, O., & Wiik, J. E. 2003, Sol. Phys., 216, 109
Lin, Y., Engvold, O., Rouppe van der Voort, L. H. M., Wiik, J. E., & Berger, T. E. 2005, Sol. Phys., 226, 239
Lin, Y., Engvold, O., Rouppe van der Voort, L. H. M., & van Noort, M. 2007, Sol. Phys., 246, 65
Lin, Y., Martin, S. F., & Engvold, O. , et al. 2008, in ASP Conf. Ser. 383, Subsurface and Atmospheric Influences on Solar Activity, ed. R. Howe et al. (San Francisco: ASP), 235
Luna, M., Terradas, J., Oliver, R., & Ballester, J. L. 2008, ApJ, 676, 717
Luna, M., Terradas, J., Oliver, R., & Ballester, J. L. 2009, ApJ, 692, 1582
Molowny-Horas, R., Wiehr, E., Balthasar, H., Oliver, R., & Ballester, J. L. 1999, JOSO Annual Report 1998, Astron. Inst. Tatranska Lomnica, 126
Okamoto, T. J, et al. 2007, Science, 318, 1557
Oliver, R., & Ballester, J. L. 2002, Sol. Phys., 206, 45
Rempel, M., Schmitt, D., & Glatzel, W. 1999, A&A, 343, 615
Schmitt, D., & Degenhardt, U. 1995, Rev. Mod. Astron., 8, 61
Soler, R., Oliver, R., & Ballester, J. L. 2007, A&A, 471, 1023
Soler, R., Oliver, R., & Ballester, J. L. 2008, ApJ, 684, 725 (Paper I)
Terradas, J., Arregui, I., Oliver, R., & Ballester, J. L. 2008, ApJ, 678, L153
Terradas, J., Molowny-Horas, R., Wiehr, E., Balthasar, H., Oliver, R., & Ballester, J. L. 2002, A&A, 393, 637
Terra-Homem, M., Erdélyi, R., & Ballai, I. 2003, Sol. Phys., 217, 199
van Doorsselaere, T., Ruderman, M. S., & Robertson, D. 2008, A&A, 485, 849
Yi, Z., & Engvold, O. 1991, Sol. Phys., 134, 275
Yi, Z., Engvold, O., & Kiel, S. L. 1991, Sol. Phys., 132, 63
Zirker, J. B., Engvold, O., & Yi, Z. 1994, Sol. Phys., 150, 81
Zirker, J. B., Engvold, O., & Martin, S. F. 1998, Nature, 396, 440